Sr-Site Deficient La-Sm Co-Doped $SrTiO_3$ THERMOELECTRIC CERAMICS

Adindu C. Iyasara[1]
Felix U. Idu[2]
Amadi Ugochukwu B.[3]
[1,2]Department of Ceramic and Glass Technology
[3]Department of Science Laboratory Technology (Chemistry Research Unit)
Akanu Ibiam Federal Polytechnic, Unwana, Ebonyi State, Nigeria.
*Corresponding author's Email: acnnayerugo@gmail.com; Mobile: 08037390071

ABSTRACT

The phase, microstructural and thermoelectric properties of $Sr_{1-3x/2}Sm_{x/2}TiO_3$ ($0.05 \leq x \leq 0.30$) ceramics were investigated. Samples with varying concentrations of La^{3+} and Sm^{3+} ions were batched, synthesized by solid state reaction (SSR) method, calcined in air and sintered in 5 % H_2/N_2 at 1773 K for 6 h. The particle size distribution (PSD) showed mean particle size (d_{50}) of 6.0 µm while the surface morphology images from the scanning electron microscopy (SEM) revealed homogenous grain structures with average grain size of 15.3 µm. The lowest total thermal conductivity, k at 573 K was observed in x = 0.30 (3.46 W/m.K), which decreased to a minimum of 2.99 W/m.K for all the compositions at 973 K. k decreased with increasing temperature over the measured temperature range, which suggests a typical thermal conduction behaviour of a semiconductor. Overall, x = 0.30 showed the highest thermoelectric figure of merit, ZT = 0.25 at 973 K.

Keywords
Thermoelectrics, Solid-state reaction, Particle size, Grain structure, Thermal conductivity, Sr-vacancy.

INTRODUCTION

The most studied thermoelectric semiconducting materials with optimised ZT values of 1 or higher are primarily non-oxides such as $(Bi,Sb)_2(Te,Se)_3$, SiGe, PbTe and $LaFe_3CoSb_{12}$ and their corresponding alloys (Tian et al., 2014). The high ZT values are achievablemainly because they possess small phonon group velocity and low thermal conductivity *k*, desirable for thermoelectric applications. The broad application of these materials is limited, however, due to toxicity, scarcity, cost, and limited operational temperature range (Liu et al., 2013). There is evidence, however, that transition-metal oxide thermoelectric materials are viable alternatives that if given improvements in ZT, may surmount the challenges associated with non-oxides (Koumoto & Terasaki, 2006; Li et al., 2010). Among these oxide based TE materials, p-type layered cobaltates such as $NaCo_2O_4$, $(Sr,Ca)_3Co_4O_9$, $Bi_{2-x}Pb_xCo_2O_8$ ($0 \leq x \leq 0.4$), $Tl_{0.4}[Sr_{0.9}O]_{1.12}CoO_2$ and $[Pb_{0.7}Hg_{0.4}Sr_{1.9}Co_{0.2}][CoO_2]_{1.8}$ are promising with ZT = 0.8 – 1.0 at 800 – 1000 K (Lu, 2016). n-type oxides are considered inferior when compared to these p-type oxides as a result of their lower ZT values. Potential thermoelectric n-type oxide ceramics include $SrTiO_3$, $CaMnO_3$, In_2O_3 and ZnO. The highest ZT values so far reported for polycrystalline n-type oxides are 0.47 at 1000 K (Košir et al., 2017; Ohtaki et al., 2009) and 0.65 at 1247 K (Košir et al., 2017) for Al-Ga co-doped ZnO and recently ZT ≥ 0.60 at 1000 – 1100 K for 10 mol % La and 10 mol% Nb co-doped $SrTiO_3$ (J. Wang et al., 2017). Most of the thermoelectric (TE) research reported for reduced rare earth (RE) doped $SrTiO_{3-\delta}$ relate to electronic compensation mechanism (Kovalevsky, Yaremchenko, Populoh, Thiel, et al., 2014; Kovalevsky, Yaremchenko, Populoh, Weidenkaff, et al., 2014), while ionic

compensation mechanism (cation vacancy) mostly on A-site are sparingly reported (Han, Sun, Li, et al., 2017; Kovalevsky, Yaremchenko, Populoh, Weidenkaff, et al., 2014; Lu et al., 2016). Moreover, there are several reported studies of dual doped $SrTiO_3$ with La and Dy or Yb (Han, Sun, Li, et al., 2017; Liu et al., 2013; Tian et al., 2014), La and Ba (Muta et al., 2004), La and Nb or W (Popuri et al., 2014; J. Wang et al., 2017) . There is no report in the literature for $SrTiO_3$ dual doped with Sm and a second cation save our previously reported work (Iyasara et al., 2017).

Co-doping has been suggested to enhance thermoelectric properties of $SrTiO_3$ ceramics. For example, a study of La-Dy co-doped Sr-deficient $SrTiO_3$ ceramics upholds potency of dual doping and Sr vacancies in improving the efficiency of ceramics. $La_{0.1}Dy_xSr_{1-1.25(0.1+x)}TiO_3$ (x = 0, 0.05, 0.075, 0.1) ceramics were prepared using sol-gel method and sintered in 5% H_2-95% N_2 reducing gas (Han, Sun, & Song, 2017).Increase in carrier concentration due to the La-Dy co-doping improved the electrical conductivity. Sr vacancies and the generated second phase ($Dy_2Ti_2O_7$) led to promotion of phonon scattering and decrease in total thermal conductivity, k (1.92 W/m.K at 773 K) and improved ZT = 0.29 at 773 K for x = 0.1 ceramics. La-Dy co-doped ceramics, $La_{0.1}Sr_{0.83}Dy_{0.07}TiO_3$ (H C Wang et al., 2010) resulted in a reduced k (2.5 W/m.K) and a high ZT = 0.36 at 1045 K. La-Nb co-doped $SrTiO_3$ ceramics have shown to be one of the best n-type oxide thermoelectric materials. In the study of La-Nb co-doped $SrTiO_3$, a significant improved power factor and Seebeck coefficient when compared to La-doped $SrTiO_3$ was obtained which is attributed to energy filtering effect of grain boundaries (Y. Wang et al., 2013). The ZT $\geq$ 0.6 at 1000 – 1100 K for La -Nb (La10Nb10) co-doped bulk $SrTiO_3$ ceramics has been reported (J. Wang et al., 2017) which remains the highest value for bulk $SrTiO_3$ to date.

The aim of this research is to study the structural and thermoelectric properties of Sr-deficient co-doped $SrTiO_3$ using La^{3+} and Sm^{3+} cations. These cations (La^{3+} and Sm^{3+}) were utilised to validate the findings that mass contrast and nano-scale intergrowths could influence the thermal conductivity (Khaliq et al., 2015). It is also in furtherance to test the proposition that $SrTiO_3$ doped with large RE ions (e.g., La, Nd) exhibit large power factor (Dawson et al., 2013), while those doped with mid-sized or small RE ions (Sm, Gd, Dy, Er and Yb) show low k without disrupting the electrical properties (Dawson et al., 2013; Liu et al., 2013).

MATERIALS AND METHODS

A solid-state reaction method was used to prepare $Sr_{1-3x/2}Sm_{x/2}TiO_3$ ceramics from $SrCO_3$ (99.90 %, Sigma-Aldrich, UK), La_2O_3 (99.99 %, Sigma-Aldrich, UK), Sm_2O_3 (99.90 %, Stanford Materials Corporation, USA) and TiO_2 (99.90 %, Sigma-Aldrich, UK) as starting materials. These starting powders were dried and stoichiometric amounts mixed using a ball mill in isopropanol with 10 mm diameter yttria-stabilised zirconia (YSZ) milling media for 24 h. The slurry was dried at 80^{o}C, sieved through a 250 μm mesh and calcined at 1573 K in air for 6 h in alumina crucible (Boston et al., 2017). Particle size analysis (PSA) of the calcined powders was performed using a Mastersizer 3000 laser particle size analyser (Malvern Instruments Limited, UK). The calcined powers were pressed into a 20 mm diameter (with thickness $\leq$ 2 mm) disc pellet in a uniaxial press using 32 MPA of applied load for ~ 1 minute. Finally, the green pellets were sintered in flowing 5 % H_2/N_2 gas at a cooling rate of 10 ^{o}C/min at 1773 K for 6 h. The sintered ceramics were wet polished to remove surface impurities and produce smooth (and flat) surface samples (Iyasara et al., 2017). The experimental density of the ceramics was determined by applying Archimedes principle using an electronic digital density balance (Mettler-Toledo AG Balance). Thermogravimetric analysis (TGA) to determine the rate of oxygen uptake (weight variation) and thermal stability of ceramics in air at room temperature to 1000 ^{o}C was carried out using Perkin Elmer Pyris 1 TGA computer-controlled analyser.

Phase analysis of ceramics was carried out by powder x-ray diffraction (XRD) with Cu Kα radiation (λ = 1.5406 Å) using a D2 phase diffractometer. The scan was conducted across the 2θ range of 20 – 80 degrees with a step size of 0.02° at a scan rate of 1°/min. Phase identity and purity of the collected data were analysed using the ICDD Sleve + PDF-4+ software. Ceramic samples for microstructural examination were ground, polished using a diamond polishing wheel and thermally etched. The microstructures were studied using a Philips XL 30 S-FEG scanning electron microscope. The average grain size in the microstructures was calculated using the line-intercept method (Chan et al., 2017) after Mendelson method (Mendelson .MI, 1969). Seebeck coefficient (S) and electrical conductivity (σ) of ceramics were measured simultaneously on 20 mm disc pellets in Ar atmosphere from 573-973 K using Netzsch SBA 458 Nemesis Seebeck coefficient and electrical conductivity analyser. Thermal conductivity measurements were performed using Anter Flashline TM 3000 thermal properties analyser with a high-speed xenon discharge (HSXD) pulse source on 10 x 10 mm^2 samples.

RESULTS AND DISCUSSION

Phase analysis

Figure 1 shows the room temperature XRD patterns of $Sr_{1-3x/2}La_{x/2}Sm_{x/2}TiO_3$ ceramics sintered in 5% H_2/N_2 at 1773 K for 6 h. All the major peaks can be indexed with the $SrTiO_3$ cubic perovskite structure belonging to the Pm-3m space group. No secondary phase was detected within the limits of the diffractometer. The lattice parameters, cell volumes and theoretical densities were calculated from the XRD data and results are shown in Table 1. The dopant (La-Sm) concentration dependence of the lattice parameters of the ceramics are presented in Figure 2.

The lattice parameters of the compositions show a progressive decreasing relationship with increasing La-Sm concentrations (Figure 2). The lattice parameters contract from 3.910 Å (for x = 0.05) to a minimal value of 3.902 Å for x = 0.30. The decrease in lattice parameter is attributed to the smaller ionic radii of La^{3+} and Sm^{3+} (La^{3+} = 1. 36 Å; Sm^{3+} = 1.24 Å in Coordination Number, CN 12) than that of Sr^{2+} ionic radius (1.44 Å in CN 12) (Liu et al., 2013; Lu et al., 2016; H C Wang et al., 2010) and in obedience to Vegard's law.

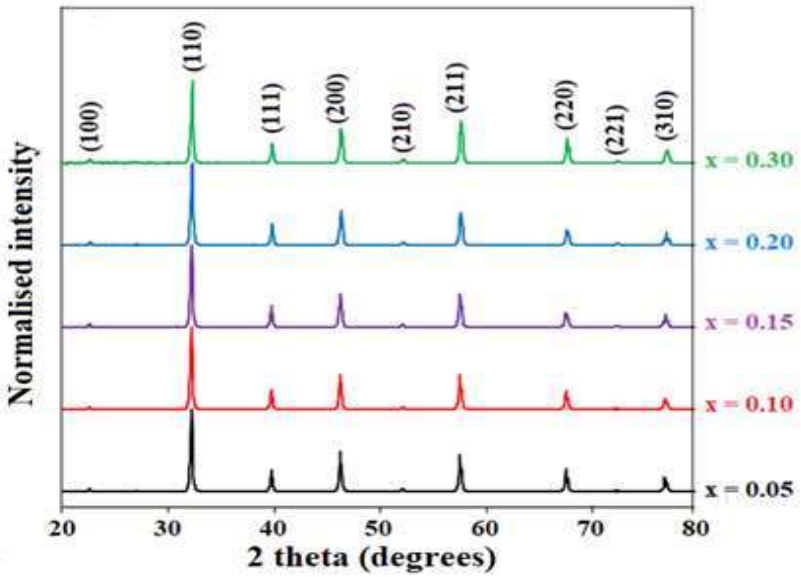

Figure 1. Room temperature XRD patterns for $Sr_{1-3x/2}La_{x/2}Sm_{x/2}TiO_3$; 0.05 ≤x ≤ 0.30 ceramics sintered in 5% H_2/N_2 at 1773 K for 6 h.

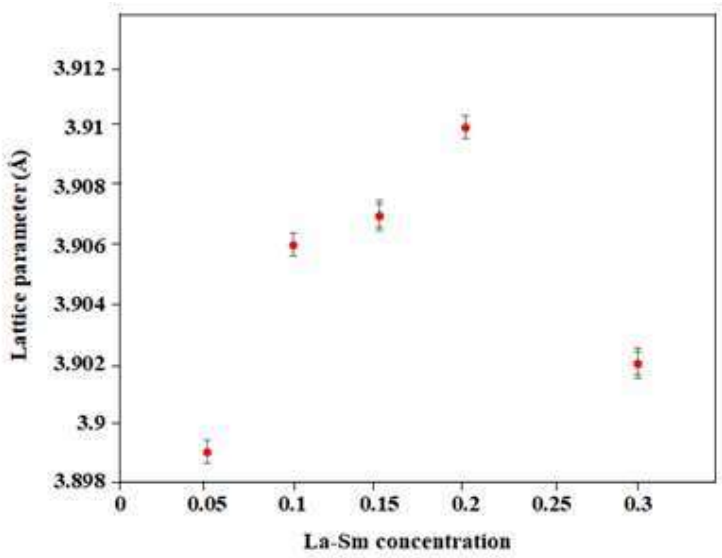

Figure 2. Dopant (La-Sm) concentration dependence of the lattice parameters of $Sr_{1-3x/2}La_{x/2}Sm_{x/2}TiO_3$; $0.05 \leq x \leq 0.30$.

Table 1. Lattice parameters, cell volumes and theoretical densities of $Sr_{1-3x/2}La_{x/2}Sm_{x/2}TiO_3$; $0.05 \leq x \leq 0.30$ ceramics sintered in 5% H_2/N_2 at 1773 K for 6 h.

Composition x	Lattice parameter (Å) (±0.001 Å)	Cell volume (Å) (±0.002 Å)	Relative density (%) (±0.5 %)
0.05	3.91	59.776	96.4
0.10	3.909	59.731	98.9
0.15	3.907	59.639	98.2
0.20	3.903	59.639	98.4
0.30	3.902	59.410	98.9

Particle size and grain structure

Particle size distribution (PSD) of calcined Sr-site deficient La-Sm co-doped $SrTiO_3$ powders after ball milling is presented in Table 2. All milled powders have mean particle size (d_{50}) $\leq$ 6 µm and d_{90} (90 % of sample particles) $\leq$ 12 µm. (Lu, 2016) worked on similar powder (La-doped $SrTiO_3$) using attrition milling and obtained much smaller particles ($d_{50} \leq 3$ µm and $d_{90} \leq 9$ µm). This confirms the postulation of (Boston et al., 2017) that attrition milling utilising high energy mixing is more efficient than ball milling in reducing particle size. However, attrition milling has a higher possibility of introducing impurities such as ZrO_2 into the reaction from the milling media (Boston et al., 2017).

Table 2. Particle sizes of calcined La-Sm co-doped $SrTiO_3$ powders after 24 h ball milling.

Composition	x	Particle diameter (μm)		
		d_{10}	d_{50}	d_{90}
$Sr_{1-3x/2}La_{x/2}Sm_{x/2}TiO_3$	0.05	2.2	4.9	12.4
	0.10	2.4	5.0	9.8
	0.15	2.7	5.6	10.7
	0.20	2.9	6.0	11.5
	0.30	2.0	4.3	10.4

Secondary electron microscopy (SEM) micrographs of the thermally etched, carbon coated surfaces for $Sr_{1-3x/2}La_{x/2}Sm_{x/2}TiO_3$ ceramics are shown in Figures 3. All compositions showed a relative density of ≥ 96 % (Table 2). All images revealed homogenous and dense microstructures consistent with their high relative density. In addition, all samples exhibited regular polygonal-shaped grain structures, with size increasing with doping concentration. The average grain size of the ceramics increased from 5.1 μm (for x = 0.05) to 9.6, 14.9 and 15.3 μm for x = 0.10, 0.20 and 0.30 ceramics, respectively.

Artefacts (labelled with white circles on the images) were observed on the grain and grain boundaries of the SEM images. This abnormal feature is likely deposited onto the ceramics through sample preparations or absorbed dirt or trapped impurities in the furnaces used for the processing. These impurities are more pronounced in x = 0.30, and with enlarged sizes. Since the presence of impurities and defects affect k, these artefacts might have contributed to the low thermal conductivity observed in this composition.

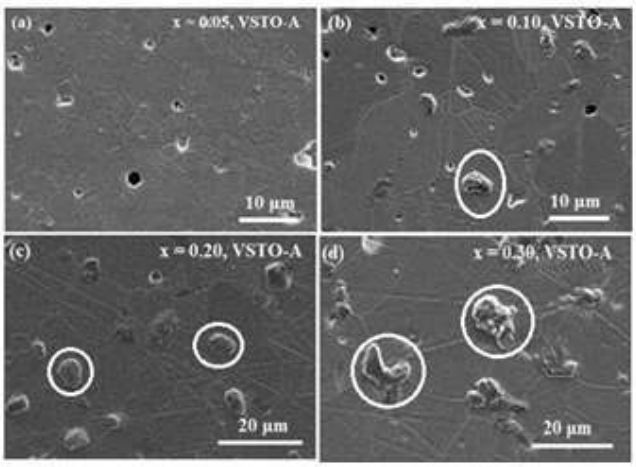

Figure 3. SEM micrographs of the surfaces of $Sr_{1-3x/2}La_{x/2}Sm_{x/2}TiO_3$ ceramics sintered at 1773 K for 6 h in 5% H_2/N_2. Observed artefacts are labelled with white circles.

Thermogravimetric analysis

In all samples, oxygen uptake increased with increasing La-Sm concentration and decreased with oxidation temperature (Figure 4). x = 0.05 were stable in air up to 1000 ^{o}C. x = 0.05 were stable in air up to 1000 ^{o}C. The colour of the ceramics after TGA remained black for x ≤ 0.10, turned to brown for x ≤ 0.20 and white for x = 0.30. All the ceramics after TGA remained stable up to 475 ^{o}C and this is within the intermediate temperature range (300 -700 ^{o}C), suggested as desirable for a ceramic-based TE generator technology (Boston et al., 2017).

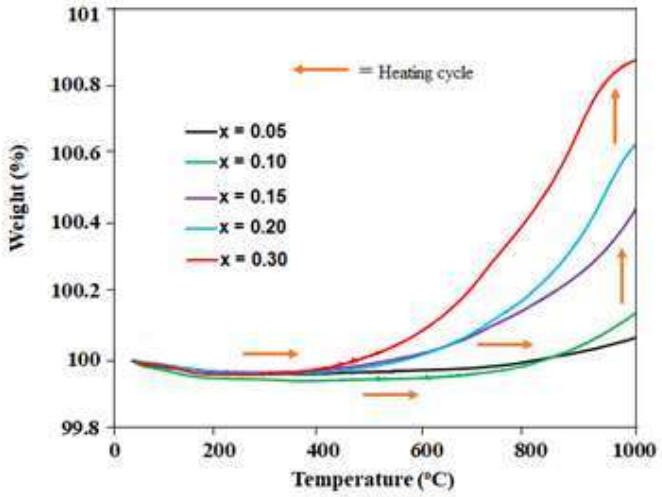

Figure 4. Thermogravimetric analysis showing the oxidation in air up to 1000 ^{o}C of $Sr_{1-3x/2}La_{x/2}Sm_{x/2}TiO$ceramics sintered in 5% H_2/N_2 at 1773 K for 6 h.

Table 3. TGA result showing the weight variation and oxidation onset temperature of $Sr_{1-3x/2}La_{x/2}Sm_{x/2}TiO_3$ ceramics sintered in 5% H_2/N_2 at 1773 K for 6 h.

Composition x	Weight change Δwt. (%)	Oxidation onset temperature (°C)
0.05	0.00	> 1000
0.10	0.12	900
0.15	0.41	600
0.20	0.62	600
0.30	0.87	520

Thermoelectric properties

The σ, $|S|$, PF, k, k_L, k_E and ZT for $Sr_{1-3x/2}La_{x/2}Sm_{x/2}TiO_3$ ceramics sintered at 1773 K for 6 h in 5% H_2/N_2 gas over a range of different temperatures and values of x are shown in Figures 5 to 7. For all samples, electrical conductivity (σ) decreases with increasing temperature over the measured temperature range, Figure 5(a), which confirms metallic behaviour. It also implies the properties share a similar conduction mechanism (Muta et al., 2005; Hong Chao Wang et al., 2011). σ for x ≤ 0.20 compositions increases with increasing La-Sm concentration, showing the

dependence of σ on carrier concentration and mobility (Snyder & Toberer, 2008). At x = 0.30, the electrical conductivity decreased. This drop may relate to solid solution limit (though no secondary phase was observed in the XRD and SEM images) or structural phase transitions as a result of rotation of O-octahedra observed in RE-doped $SrTiO_3$(Kovalevsky, Yaremchenko, Populoh, Thiel, et al., 2014; Lu et al., 2016). The highest electrical conductivity obtained was 1184 S/cm at 573 K for x = 0.20. From literature, heavily doped La-Sm VSTO-A ceramics ($x \geq 0.15$) in this study show enhanced σ when compared to that of $Sr_{0.9}Nd_{0.1}TiO_3$ with B_2O_3 and Zr_2O_3 additions (Ekren et al., 2018) and La-Nb co-doped $SrTiO_3$ ceramics (J. Wang et al., 2017) at the same temperature range (573 - 973 K). The σ result concludes that A-site vacancy has a greater effect on conductivity than electronic compensation in La-Sm doped $SrTiO_3$ (σ_{max} = 942 S/cm at 573 K for x = 0.15)(Iyasara et al., 2017). This may relate to greater oxide ion diffusion rates through the vacated A-site which permits a greater volume of reduced material throughout the ceramic.

Seebeck coefficients of all ceramics are negative, indicating n-type conduction behaviour. Absolute coefficient, $|S|$ for all compositions, Figure 5(b) increase linearly with increasing temperature, showing a metallic behaviour (Muta et al., 2005; H C Wang et al., 2010; Hong Chao Wang et al., 2011). $|S|$ values decrease as La-Sm concentration increases, possibly due to an increase in the carrier concentration resulting in an increase in electrical conductivity as shown in Figure 5(a). The $|S|$ value of all samples at high temperature (973 K) falls within the range of 158-255 μV/K. It is noted however, that these $|S|$ values are higher than the minimum values of Seebeck coefficients (150 -250 μV/K) suggested for a good TE material (Dehkordi, 2014). In addition, the Seebeck coefficients obtained are similar to data reported for La-Dy doped $SrTiO_3$ (H C Wang et al., 2010; Hong Chao Wang et al., 2011) and La-Nb doped $SrTiO_3$ ceramics (J. Wang et al., 2017),but lower than the values reported by Ha (Han, Sun, & Song, 2017)for La-Dy co-doped Sr-deficient $SrTiO_3$ ceramics.

The power factors, PF for samples with La-Sm concentrations ranging from 15 to 30 mol% ($x \geq 0.15$) displays a peak between 573 and 673 K (Figure 5c), suggesting a semiconductor-like mechanism. Above 673 K, the power factors decreased with increasing temperature. For $x \leq 0.10$, the PF decreases in the entire measured temperature range. The maximum PF value of ~ 1185 $\mu W/K^2$ for x = 0.10 at 573 K was obtained. This high PF could be attributed to an optimised $|S|$ recorded (125-193 μV/K) which is higher than the $|S|$ values of other compositions except x = 0.05. However, at high temperatures, the PF of x = 0.10 decreased, and could be due to the low σ exhibited, Figure 5(a). The PF results obtained in this study are in agreement with most results in the literature for electron La-Yb (H. Wang & Wang, 2013) and La-Dy (H C Wang et al., 2010; Hong Chao Wang et al., 2011) co-doped $SrTiO_3$ ceramics, but higher than the reported values for Nb-doped $Sr_{0.95}La_{0.05}TiO_3$ ceramics at high temperatures (≥ 973 K) (H C Wang et al., 2009). Although the power factors obtained in this study are not as high as the values observed in La-Nb doped $SrTiO_3$ reported by (J. Wang et al., 2017) and in doped $SrTiO_3$ single crystals (Ohta et al., 2005; Okuda et al., 2001),the maximum PF recorded is among the high levels in polycrystalline $SrTiO_3$ bulk ceramics.

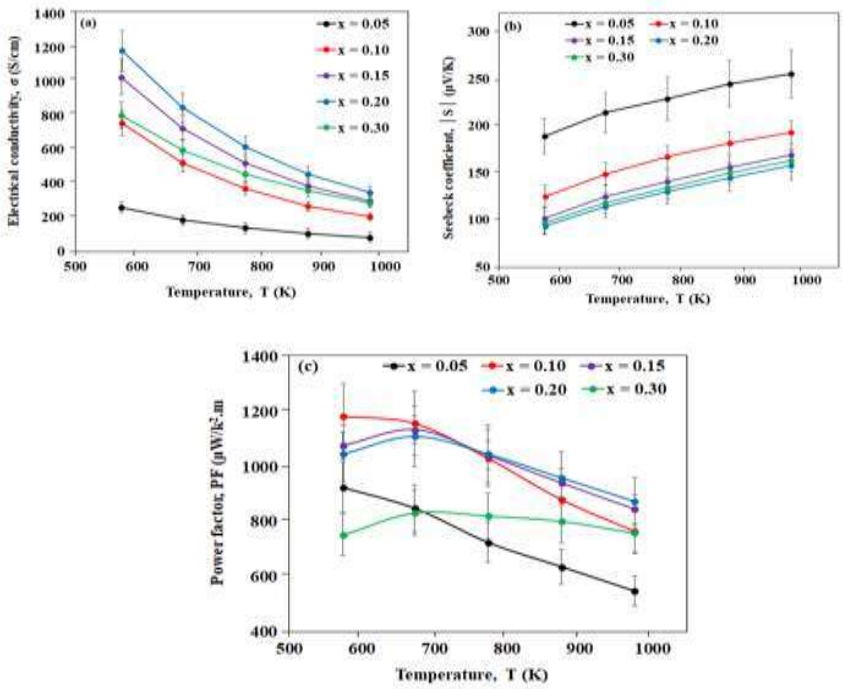

Figure 5. Temperature dependence of (a) electrical conductivity, σ (b) Seebeck coefficient, $|S|$ (c) power factor, PF for $Sr_{1-3x/2}La_{x/2}Sm_{x/2}TiO_3$ ceramics sintered in 5% H_2/N_2 at 1773 K for 6 h.

The highest total thermal conductivity, k (5.57 W/m. K) at 573 K was observed in x = 0.10, Figure 6(a). In contrast, the lowest k at 573 K was observed in x = 0.30 (3.46 W/m.K), which decreases to a minimum of 2.99 W/m.K for all the compositions at 973 K. Total thermal conductivity decreases with increasing temperature over the measured temperature range, which suggests a typical thermal conduction behaviour of a semiconductor (Hong Chao Wang et al., 2011) and domination of lattice thermal conductivity k_L (H. Wang & Wang, 2013), Figure 6(b). The high concentration of impurities in the microstructure of x = 0.30 ceramics may have affected the thermal transport, leading to the low k observed. Generally, the reduction of k in doped $SrTiO_3$ ceramics is ascribed to formation of V_O in perovskites, preceded by sintering in reducing atmosphere (Kovalevsky, Yaremchenko, Populoh, Thiel, et al., 2014). An increase in La-Sm concentration results in decreasing k_L, which indicates increasing lattice defects and shortening of the mean free path (MFP) of phonons resulting to low k (Lu et al., 2016). At the maximum temperature (973 K), the electronic contribution to the total thermal conductivity was estimated at 0.20 W/m. K (5.1%), 0.49 W/m. K (12.8%), 0.71 W/m. K (18.8%), 0.84 W/m. K (20.9%), 0.68 W/m. K (22.8%) for x = 0.05, 0.10, 0.15, 0.20 and 0.30, respectively. From the results of the thermal transport properties, it can be deduced the reduction in k mainly emanates from the lattice vibrations (phonons), hence k_L plays a dominant role in k.

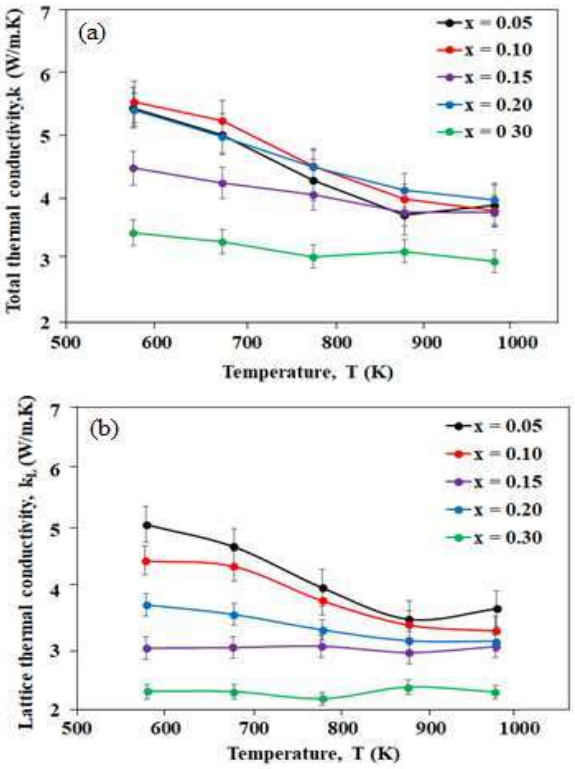

Figure 6. Temperature dependence of (a) total thermal conductivity, k (b) lattice thermal conductivity, k_L for $Sr_{1-3x/2}La_{x/2}Sm_{x/2}TiO_3$ ceramics sintered in 5% H_2/N_2 at 1773 K for 6 h.

The thermoelectric figure of merit, ZT of all the compositions increases with increasing temperature over the entire measured temperature range as shown in Figure 7. By optimising the La-Sm doping concentration, x = 0.30 recorded the highest ZT value of 0.25 at 973 K. However, the highest ZT value did not occur in x = 0.20 sample which have both the highest electrical conductivity (350 S/cm at 973 K), Figure 5(a) and power factor (873 $\mu W/K^2.m$ at 973 K), Figure 5(c) values as expected. Obviously, the dramatic decrease observed in the k of x = 0.30 sample despite its low PF results in higher ZT values especially at high temperatures (773 – 973 K). This suggests that heavy doping ($x \geq 0.30$) of A-site vacancy $Sr_{1-3x/2}La_{x/2}Sm_{x/2}TiO_3$ ceramics has less effect in enhancing the electrical transport properties especially the power factor.

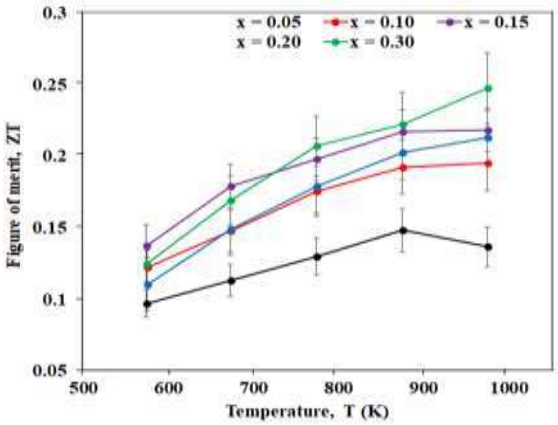

Figure 7. Temperature dependence of thermoelectric figure of merit, ZT for $Sr_{1-3x/2}La_{x/2}Sm_{x/2}TiO_3$ ceramics sintered in 5% H_2/N_2 at 1773 K for 6 h.

CONCLUSIONS

Ionically co-doped $SrTiO_3$ using La^{3+} and Sm^{3+} cations with a resultant maximum ZT of 0.25 at 973 K were presented. The obtained results discussed in this study showed La-Sm co-doped $SrTiO_3$ TE ceramics can be improved via creation of Sr-vacancy. In comparison with our previous work (Iyasara et al., 2017) and related works in the literature, co-doping had a minimal effect on k leading to the conclusion that optimising ZT by this method is of limited value. However, the suggested batched stoichiometries which favour the formation of A-site deficiencies with a view to optimising the ZT had an insignificant effect on the studied ceramics.

▪ REFERENCES

Boston, R., Schmidt, W. L., Lewin, G. D., Iyasara, A. C., Lu, Z., Zhang, H., Sinclair, D. C., & Reaney, I. M. (2017). Protocols for the fabrication, characterization, and optimization of n-type thermoelectric ceramic oxides. *Chemistry of Materials*, *29*(1). https://doi.org/10.1021/acs.chemmater.6b03600

Chan, J. H., Bock, J. A., Guo, H., Trolier-McKinstry, S., & Randall, C. A. (2017). High-temperature thermoelectric characterization of filled strontium barium niobates: power factors and carrier concentrations. *Journal of Materials Research*, *32*(06), 1160–1167. https://doi.org/10.1557/jmr.2017.18

Dawson, J. A., Li, X., Freeman, C. L., Hardinga, J. H., & Sinclair., D. C. (2013). The application of a new potential model to the rare-earth doping of $SrTiO_3$ and $CaTiO_3$. *Journal of Materials Chemistry C*, *1*(8), 1574–1582. https://doi.org/10.1039/c2tc00475e

Dehkordi, A. M. (2014). *An Experimental Investigation Towards Improvement of Thermoelectric Properties of Strontium Titanate Ceramics*. Clemson University.

Ekren, D., Azough, F., Gholinia, A., Day, S. J., Hernandez-Maldonado, D., Kepaptsoglou, D. M., Ramasse, Q. M., & Freer, R. (2018). Enhancing the thermoelectric power factor of $Sr_{0.9}Nd_{0.1}TiO_3$ through control of the nanostructure and microstructure. *Journal of Materials Chemistry A*, *6*(48), 24928–24939. https://doi.org/10.1039/c8ta07861k

Han, J., Sun, Q., Li, W., & Song, Y. (2017). Microstructure and thermoelectric properties of $La_{0.1}Dy_{0.1}SrxTiO_3$ ceramics. *Ceramics International*, *43*(7), 5557–5563. https://doi.org/10.1016/j.ceramint.2017.01.083

Han, J., Sun, Q., & Song, Y. (2017). Enhanced thermoelectric properties of La and Dy co-doped, Sr-deficient $SrTiO_3$ceramics. *Journal of Alloys and Compounds*, *705*, 22–27. https://doi.org/10.1016/j.jallcom.2017.02.146

Iyasara, A. C., Schmidt, W. L., Boston, R., Sinclair, D. C., & Reaney, I. M. (2017). La and Sm Co-doped $SrTiO_{3-\delta}$ Thermoelectric Ceramics. *Materials Today: Proceedings*, *4*(12), 12360–12367. https://doi.org/10.1016/j.matpr.2017.10.004

Khaliq, J., Chunchun, L., Kan, C., Baogui, S., Haitao, Y., Grande, A. M., Yan, H., & Reece, M. J. (2015). Reduced thermal conductivity by nanoscale intergrowths in perovskite like layered structure $La_2Ti_2O_7$. *Journal of Applied Physics*, *117*(7), 2–8. https://doi.org/10.1063/1.4908209

Košir, M., Podlogar, M., Daneu, N., Rečnik, A., Guilmeau, E., & Bernik, S. (2017). Phase formation, microstructure development and thermoelectric properties of $(ZnO)_kIn_2O_3$ ceramics. *Journal of the European Ceramic Society*, *37*(8), 2833–2842. https://doi.org/10.1016/j.jeurceramsoc.2017.03.019

Koumoto, K., & Terasaki, I. (2006). Complex Oxide Materials for Thermoelectric Applications. *MRS Bulletin*, *31*(March), 206–210. https://doi.org/10.1557/mrs2006.46

Kovalevsky, A. V., Yaremchenko, A. A., Populoh, S., Thiel, P., Fagg, D. P., Weidenkaff, A., & Frade, J. R. (2014). Towards a high thermoelectric performance in rare-earth substituted $SrTiO_3$: effects provided by strongly-reducing sintering conditions. *Phys. Chem. Chem. Phys.*, *16*(48), 26946–26954. https://doi.org/10.1039/C4CP04127E

Kovalevsky, A. V., Yaremchenko, A. A., Populoh, S., Weidenkaff, A., & Frade, J. R. (2014). Effect of A-site cation deficiency on the thermoelectric performance of donor-substituted strontium titanate. *Journal of Physical Chemistry C*, *118*(9), 4596–4606. https://doi.org/10.1021/jp409872e

Li, J. F., Liu, W. S., Zhao, L. D., & Zhou, M. (2010). High-performance nanostructured thermoelectric materials. *NPG Asia Materials*, *2*(4), 152–158. https://doi.org/10.1038/asiamat.2010.138

Liu, J., Wang, C. L., Li, Y., Su, W. B., Zhu, Y. H., Li, J. C., & Mei, L. M. (2013). Influence of rare earth doping on thermoelectric properties of $SrTiO_3$ ceramics. *Journal of Applied Physics*, *114*(22). https://doi.org/10.1063/1.4847455

Lu, Z. (2016). La doped $SrTiO_3$ Based Oxide Thermoelectrics. [University of Sheffield]. In *University of Sheffield.* http://etheses.whiterose.ac.uk/id/eprint/11817

Lu, Z., Zhang, H., Lei, W., Sinclair, D. C., & Reaney, I. M. (2016). High-Figure-of-Merit Thermoelectric La-Doped A-Site-Deficient $SrTiO_3$ Ceramics. *Chemistry of Materials*, *28*(3), 925–935. https://doi.org/10.1021/acs.chemmater.5b04616

Mendelson .MI. (1969). Average Grain Size in Polycrystalline Ceramics. *Journal of the American Ceramic Society*, *52*(8), 443–446. https://doi.org/10.1111/j.1151-2916.1969.tb11975.x

Muta, H., Kurosaki, K., & Yamanaka, S. (2004). Thermoelectric properties of doped $BaTiO_3$-$SrTiO_3$ solid solution. *Journal of Alloys and Compounds*, *368*(1–2), 22–24. https://doi.org/10.1016/j.jallcom.2003.07.016

Muta, H., Kurosaki, K., & Yamanaka, S. (2005). Thermoelectric properties of reduced and La-doped single-crystalline $SrTiO_3$. *Journal of Alloys and Compounds*, *392*(1–2), 306–309. https://doi.org/10.1016/j.jallcom.2004.09.005

Ohta, S., Nomura, T., Ohta, H., & Koumoto, K. (2005). High-temperature carrier transport and thermoelectric properties of heavily La- or Nb- doped single crystals. *Journal of Applied Physics*, *97*(3), 0341061–0341064. https://doi.org/10.1063/1.1847723

Ohtaki, M., Araki, K., & Yamamoto, K. (2009). High thermoelectric performance of dually doped ZnO ceramics. *Journal of Electronic Materials*, *38*(7), 1234–1238. https://doi.org/10.1007/s11664-009-0816-1

Okuda, T., Nakanishi, K., Miyasaka, S., & Tokura, Y. (2001). Large Thermoelectric Response of Metallic Perovskite: $Sr_{1-x}La_xTiO_3$ ($0 \leq x \leq 0.1$). *Physical Review B*, *63*, 1131041–1131044. https://doi.org/10.1103/PhysRevB.63.113104

Popuri, S. R., Scott, A. J. M., Downie, R. A., Hall, M. A., Suard, E., Decourt, R., Pollet, M., & Bos, J.-W. G. (2014). Glass-like thermal conductivity in $SrTiO_3$ thermoelectrics induced by A-site vacancies. *RSC Adv.*, *4*(64), 33720–33723. https://doi.org/10.1039/C4RA06871H

Snyder, G. J., & Toberer, E. S. (2008). Complex thermoelectric materials. *Nat Mater*, *7*(2), 105–114. https://doi.org/10.1038/nmat2090

Tian, Z., Lee, S., & Chen, G. (2014). A Comprehensive Review of Heat Transfer in Thermoelectric Materials and Devices. *Annual Review of Heat Transfer*, 1–64. https://doi.org/10.1615/AnnualRevHeatTransfer.2014006932

Wang, H., & Wang, C. (2013). Thermoelectric properties of Yb-doped $La_{0.1}Sr_{0.9}TiO_3$ ceramics at high temperature. *Ceramics International*, *39*(2), 941–946. https://doi.org/10.1016/j.ceramint.2012.07.009

Wang, H C, Wang, C. L., Su, W. B., Liu, J., Peng, H., Zhang, J. L., Zhao, M. L., Li, J. C., Yin, N., & Mei, L. M. (2009). Substitution effect on the thermoelectric properties of reduced Nb-doped. *Journal of Alloys and Compounds*, *486*, 693–696. https://doi.org/10.1016/j.jallcom.2009.07.041

Wang, H C, Wang, C. L., Su, W. B., Liu, J., Zhao, Y., Peng, H., Zhang, J. L., Zhao, M. L., Li, J. C., Yin, N., & Mei, L. M. (2010). Enhancement of thermoelectric figure of merit by doping Dy in $La_{0.1}Sr_{0.9}TiO_3$ ceramic. *Materials Research Bulletin*, *45*(7), 809–812. https://doi.org/10.1016/j.materresbull.2010.03.018

Wang, Hong Chao, Wang, C. L., Su, W. Bin, Liu, J., Sun, Y., Peng, H., & Mei, L. M. (2011). Doping effect of La and Dy on the thermoelectric properties of $SrTiO_3$. *Journal of the American Ceramic Society*, *94*(3), 838–842. https://doi.org/10.1111/j.1551-2916.2010.04185.x

Wang, J., Zhang, B. Y., Kang, H. J., Li, Y., Yaer, X., Li, J. F., Tan, Q., Zhang, S., Fan, G. H., Liu, C. Y., Miao, L., Nan, D., Wang, T. M., & Zhao, L. D. (2017). Record high thermoelectric performance in bulk $SrTiO_3$ via nano-scale modulation doping. *Nano Energy*, *35*(April), 387–395. https://doi.org/10.1016/j.nanoen.2017.04.003

Wang, Y., Zhang, X., Shen, L., Bao, N., Wan, C., Park, N. H., Koumoto, K., & Gupta, A. (2013). Nb-doped grain boundary induced thermoelectric power factor enhancement in La-doped $SrTiO_3$ nanoceramics. *Journal of Power Sources*, *241*, 255–258. https://doi.org/10.1016/j.jpowsour.2013.04.143